CHAPTER 3

Experimental Procedures

3.1 Objectives

To evaluate and compare structure-property relationship of candidate 200-series austenitic stainless steels (ASSs) to be used as an alternative to AISI 304 and/ or AISI 304L in pipe-line application where the working environment is mild corrosive without heavy loading, e.g. as drain pipe at the end of the waste process line in petrochemical industry and/or household tubular shape utensil.

3.2 Materials and Summary of Methodology

Two of 300-series reference and three candidates of 200-series ASSs were studied as given in Table 3.1. Sheets with thickness of 2 mm were utilized in PCTIGW with no filler. Methodology applied for as-received base metals and PCTIG welds is summarized in Table 3.2.

Table 3.1 Experimental Austenitic Stainless Steels

Group	Grade
Reference 300-Series	AISI 304 AISI 304L
Candidates 200-series	201-1M 201-2M AISI 202

Table 3.2 Summary of Methodology

Methodology	As-received Base ASSs	PCTIG Welds
Chemical Composition	GDS	O_2/N_2 combustion analysis (at weld-centered line)
Phase Identification	XRD	Ferritescope
Microstructure	OM SEM, EPMA	OM SEM, EPMA
Mechanical Properties	Tensile MVH	Tensile MVH
Corrosion Properties	Pitting DOS	Pitting DOS

GDS = Glow Discharge Spectrometry, XRD = X-ray Diffractometry,

OM = Optical microscopy

SEM = Scanning Electron Microscopy, EPMA = Electron Probe Microanalysis,

MVH = Micro-Vickers Hardness Test, DOS = Degree of Sensitization

3.3 Pulsed Current Tungsten Inert Gas Welding (PCTIGW)

In PCTIGW process, the current is easily controllable, making it possible to weld products with thickness ranging from 0.01 to 10 mm. Tip of tungsten electrode is usually sharpened at an angle between 15° and 120° depends on the thickness of panel. The main purpose for using a pulsed current is to gain a better control of heat transfer, hence obtaining better penetration depth and bead width within the single pass and suitable for semi-automatic control process.

Setting of controlled and variable parameters for PCTIGW in the present work was adapted from the work by Lothongkum *et al*. (1999) and Farahani *et al*. (2012) as summarized in Tables 3.3 and 3.4, respectively. To enable 201-2M to be welded with comparable structure to AISI 304, N_2 gas was introduced in the shielding gas as an austenite promoter.

Table 3.3 Controlled Parameters

Controlled Parameters	Setting
Base current (A)	60
% On Time	65
Pulse frequency (Hz)	5
Electrode specification	2 wt% Thoriate tungsten diameter: 2.4 mm, tip angle: 60 degree
Shielding gas flow rate (liter/sec)	Top: 11, Bottom: 11
Nozzle specification	Ceramic, diameter: 11 mm
Arc length (mm)	2.4
Length from electrode to nozzle (mm)	4.5
Torch angle to weld plate	90 degree
Traveling speed (mm/sec)	5
Joint configuration	bead-on-plate

Table 3.4 Variable Parameters

Variable Parameters	Setting
Pulse current (A)	130 and 160
Mixing ration (Ar: N_2) by volume percentage	100:0, 95:5 and 90:10

Layout of the workbench and welding torch position is shown in Fig. 3.1.

Heat input calculation for PCTIGW process can be obtained from Eq. 3.1:

$$Q = \left(\frac{V \times I \times 60}{S \times 1000}\right) \times Efficiency \qquad (3.1)$$

when Q = heat input (kJ/mm), V = voltage (V), I = current (A) and S = welding speed (mm/min). Efficiency depends on welding processes and is 0.8 for TIGW (Kou, 2003 and Lippold and Kotecki, 2005), so calculated heat input is given in Table 3.5.

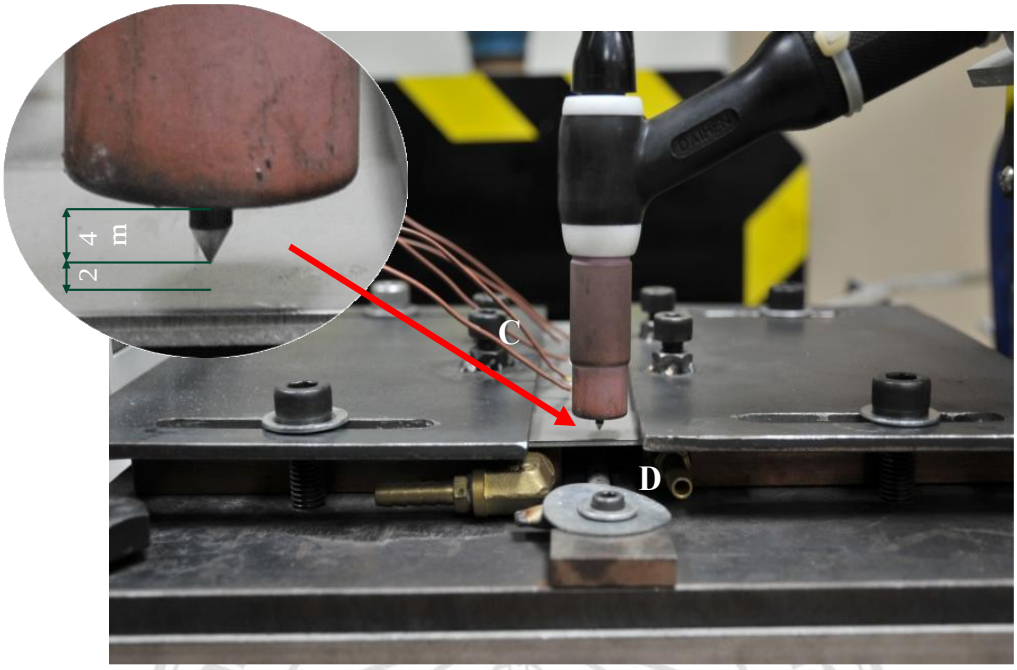

Figure 3.1 The work bench and the array of welding torch and shielding gas nozzles
A (arc length) = 2 mm, B (length from nozzle to electrode) = 4 mm,
C = thermocouples and D = bottom nozzle of shielding gas

Table 3.5 Calculated Heat Input at Various Welding Current andN_2 Percentage in Shielding Gas

Current (Amp)	**% N_2**	**Potential-1 (Volt)**	**Potential-2 (Volt)**	**Avg. Potential (Volt)**	**Heat Input (J/mm)**
130	0	10.73	10.99	10.86	168.31
	5	11.97	11.83	11.90	184.30
	10	12.37	12.36	12.37	191.57
160	0	11.90	11.78	11.84	221.71
	5	12.95	12.95	12.95	242.61
	10	13.11	13.13	13.12	245.74

To monitor temperature gradient during welding process, thermocouples have been attached to the steel plates for five points in order to monitor temperature gradients in welding cycle at the distance of 30 and 60 mm (3 and 6 cm) from the weld center line (WCL). Lay out of five thermocouples is shown in Figure 3.2.

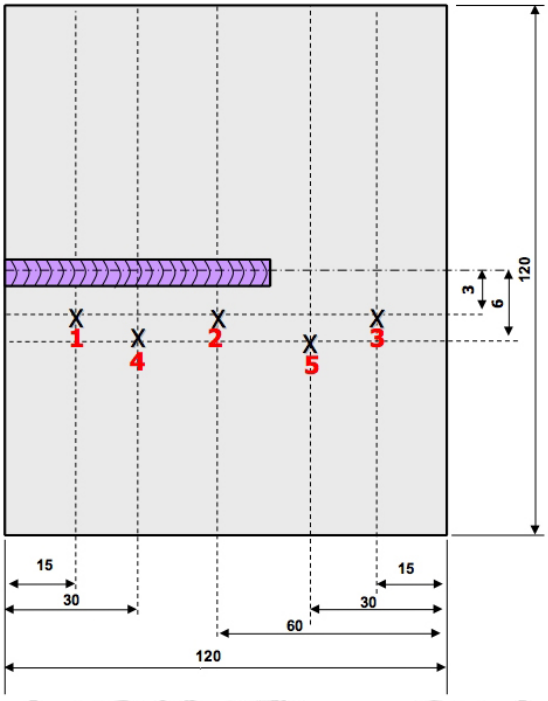

Figure 3.2 Schematic drawing showing five positions of thermocouples,attached to the weld plate

Difference in temperature gradients for welding current 130 and 160 Amp are shown in Table A1 and A2, respectively. At the distance of 3 mm from WCL, the average maximum temperature was around 800 to 900 ℃ for 130 Amp and 900 to 1100 ℃ for 160 Amp. At the distance of 6 mm from WCL, this was found to be 550 to 700 ℃ for 130 Amp and 650 to 900 ℃

Temperature difference gradient in between distant at 3 and 6 mm from WCL was around 67 ℃/mm. Therefore, the cooling rate should be rapid enough to suppress the segregation of possible precipitate phases as suggested with CCT in work of Lippold and Savage (1982).

Weld pool was inspected under optical microscope at the magnification x200 at the joint, following a procedure suggested by Prasad *et al*. (2012).

3.4 Chemical Analysis of Base Metals by Glow Discharge Spectrometry (GDS)

As-received ASS base metals are fabricated by cold-rolling and have been provided in form of 2mm roll sheet. For chemical composition analysis, base metals was cut by Struers's Exotom and Accutom-5 cutting machine into coupons, size of 30 x 30 mm2. Silicon carbide (SiC) paper grit sizes #220, 320, 500, 600, 800 and 1000 were employed for surface grinding and polishing. Test coupons were then kept in an air-tight vacuum desiccator prior to testing.

A glow discharge spectrometer (GDS), LECO GDS 850 A, was utilized for chemical composition analysis all base metals at the normal direction to the cold-rolling direction as shown in Figure 3.3.

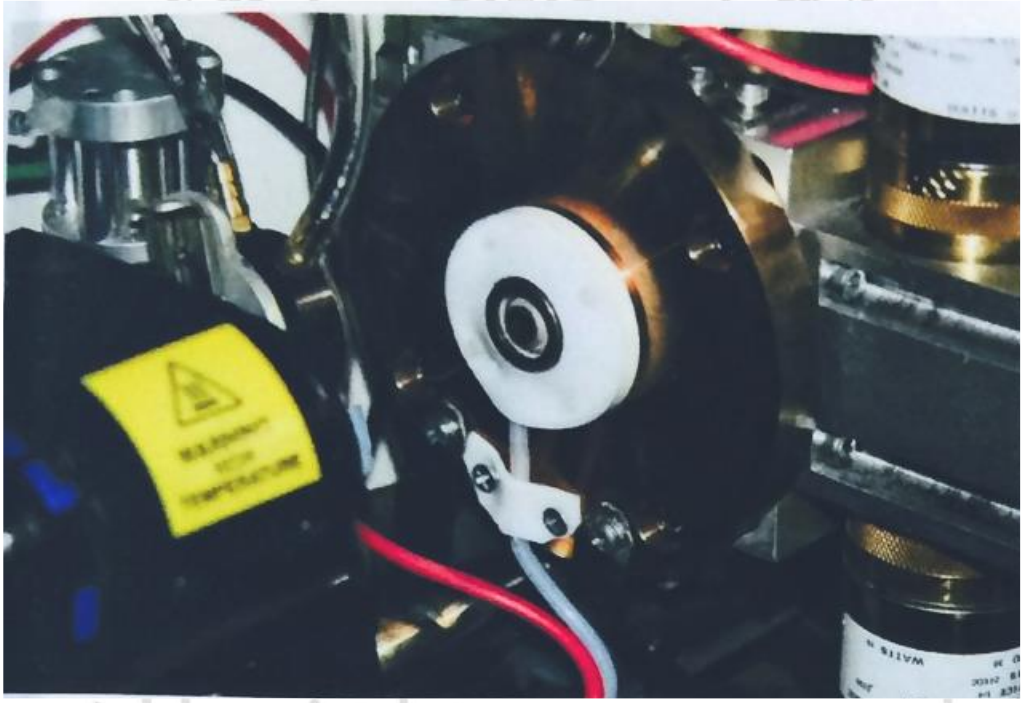

Figure 3.3 Inner chamber of glow discharge spectrometer (LECO GDS 850 A) where sample was attached

The mechanism of glow discharge (given in Figure 3.4) is that the applied potential between anode and cathode inside a gas-fill chamber forms plasma by "gas breakdown mechanism" (Bogaert and Gijbels, 1998). Positive ions and electrons in plasma are then accelerated toward the cathode material and sputtering the cathode surface to create secondary electrons entering into the plasma (Nelis and Payling, 2003).

This plasma discharge mechanism can be called “self-sustaining” and it is unique among all other emission techniques as the sputtering (sampling) mechanism is separated from the excitation and has been considered as a very clean process because there should be almost no impurity generated into the system during performing the test as compared to other techniques e.g. spark emission (Pisonero *et al*., 2006). After atoms were ejected from the cathode by plasma bombardment, they will finally return to ground state by emitting characteristic X-rays, which can be collected by photomultiplier detectors (Bogaert and Gijbels, 1998). The detected signals can then be used to quantify elemental composition as bulk analysis and as a function of erosion time to give surface profile chemical analysis of the cathode materials (Nelis and Payling, 2003).

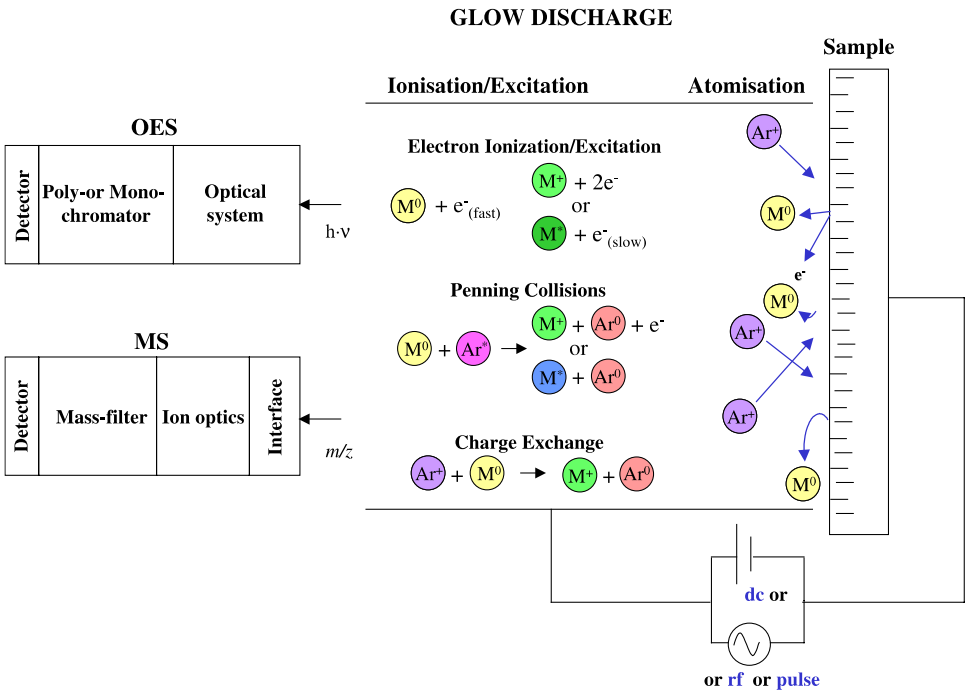

Figure 3.4 Mechanism of glow discharge spectroscopy (GDS)

(after Pisonero *et al*. (2006)

3.5 Chemical Analysis of Base Metals by Oxygen/ Nitrogen Combustion Analysis

After PCTIGW, welded specimens were inspected for the amount of nitrogen content in the weldment by an oxygen/nitrogen analyzer, Horiba EMGA-920, as shown in Figure 3.5.

Figure 3.5 Oxygen/ Nitrogen Analyzer, Horiba EMGA-920

3.6 Phase Identification by X-ray Diffractometry and Ferritscope

For base metals, typical metallographic polishing was performed as for chemical composition analysis. X-ray diffractometry was used for phase identification of base metals. Sheets were cut into coupon size of about 15 x 20 mm2 by Struer'sExotom and Accotom-5 cutting machines. A Rikaku TTRAX-III X-ray spectrometer were utilized as shown in Figure 3.6. Coupon was mounted to specimen holder. NIST SRM 640c silicon standard powder in absolute ethanol was dropped on the specimen surface as to verify peak shift position possibly caused by goniometer movement. Specimen holder was rotated at the speed of 150 rpm while operated in a 2θ range of 35 to 120 degree. Radiation source was Cu-Kα, λ = 1.5414 Angstrom. Acceleration voltage and current were 50 kV and 300 mA with a total power 15 kW. Sets of divergence (D), scattering (S) and receiving (R) slits were 1 degree, 1 degree and 0.2 radian, respectively. Step angle of 0.02 degree per second and exposure/count time of 1 second were chosen. The reason for setting XRD in continuous rotation mode was for avoiding the preferred orientation/texture effect, since cold-rolling process had been employed in fabrication of thin base-metal sheets.

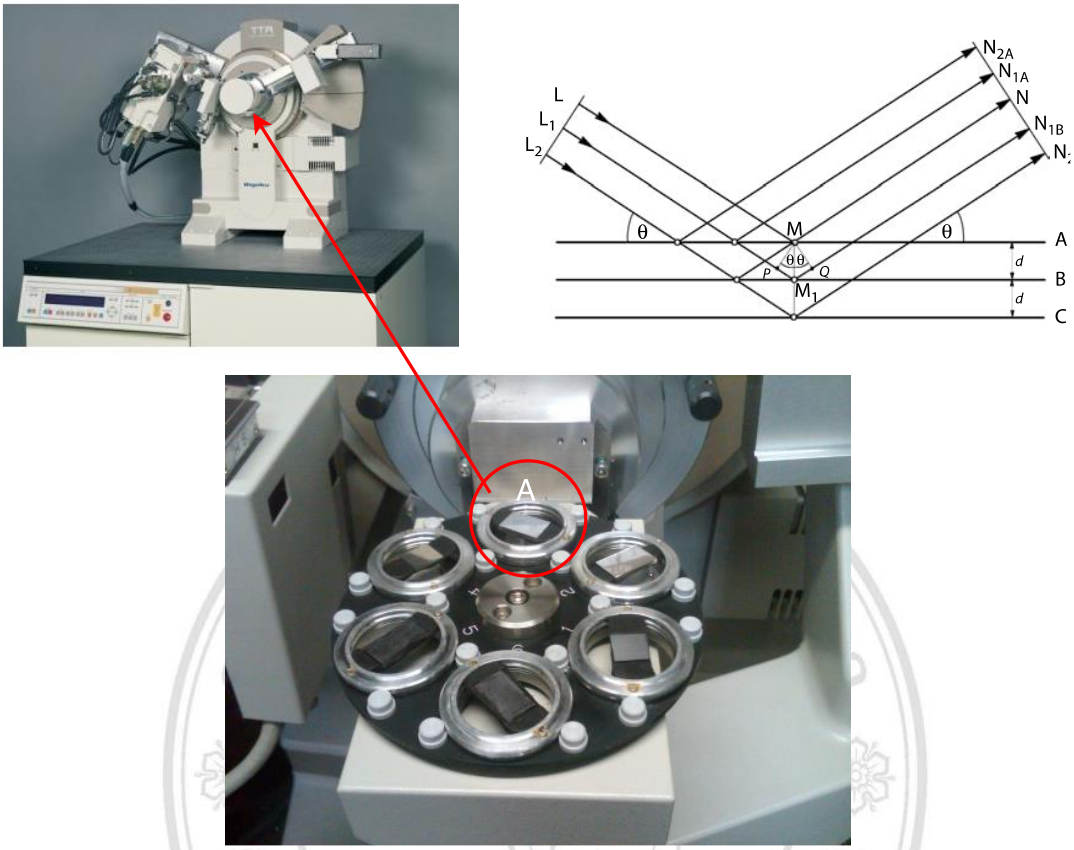

Figure 3.6 Rikaku TTRAXIII X-ray diffractometer. Diffraction pattern can be obtainedif the orientation of sample satisfied Bragg's law.

For weldment, ferrite number was determined by a Ferritescope, Fischer GmbH FMP 30, as shown in Figure 3.7.

Figure 3.7 Ferritescope, Fischer GmbH FMP 30

3.7 Microstructural Investigation by Optical Microscopy

Samples were hot-mounted in Buehler's Konductomet resin by Struers LaboPress-1 at a pressure of 20 kN and heating and cooling time of 10 and 6 minutes, respectively. After typical metallographic grinding and polishing, electro-ecthing by 2 vol% oxalic acid at an applied potential of 6 kV for 40 s was performed. An optical microscopy Olympus BH2-UMA, was utilized. Image analysis was performed by Image Pro PlusVer 5.1.0.20 software. Grain size, to be used in sensitization test as suggested by Petzow and Carle (1999), was measured by the line-intercept method per ASTM E112-08 guidance at x500 magnification, as shown in Figure 3.8.

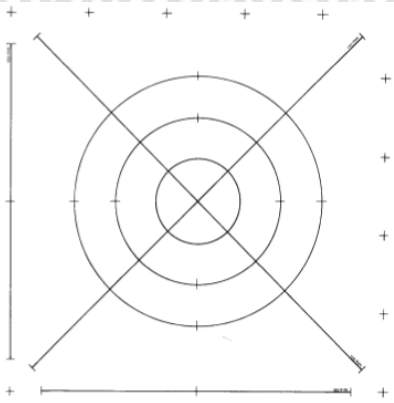

Figure 3.8 The line-intercept method per instruction in ASTM E112-08

For weldment, plan view and cross-sectional view were performed under a ZEISS Axiospolarising microscope. Measurement of width-to-depth ratio were done following the work by Kou (2003) and Prasad *et al*. (2012) using Image Pro Plus Version 5.1.0.20 software.

3.8 Microstructural Investigation by Scanning Electron Microscopy and Electron Probe Microanalysis

Samples for scanning electron microscopy (SEM) or electron probe microanalysis (EPMA) were prepared as for optical microscopy described above. JEOL-5401 and Hitachi 3400N SEMs were utilized working at accelerating voltages of 10-15 kV. Shimadzu-1610 EPMA (Figure 3.9) was used at 15 kV for both electron imaging and X-ray microanalysis.

Figure 3.9 Shimadzu-1610 EPMA

3.9 Pitting Corrosion Resistance Test

Pitting corrosion resistance test for austenitic stainless steels in the present work followed ASTM Practice G48-11, but used 3.56 wt% sodium chloride solution (pH~6.8) as electrolyte. Specimens for pitting corrosion resistance test (PCR) were prepared as coupons (15 x 15 mm2) with thickness of 2 mm. Typical metallographic grinding and polishing were performed followed the method given by Moayed *et al*. (2003). Specimens were kept at room temperature in a vacuum desiccator for at least 24 hours prior to be attached to flat cell as working electrode, labelled (B), in a typical 3-electrode cell as shown in Figure 3.10.

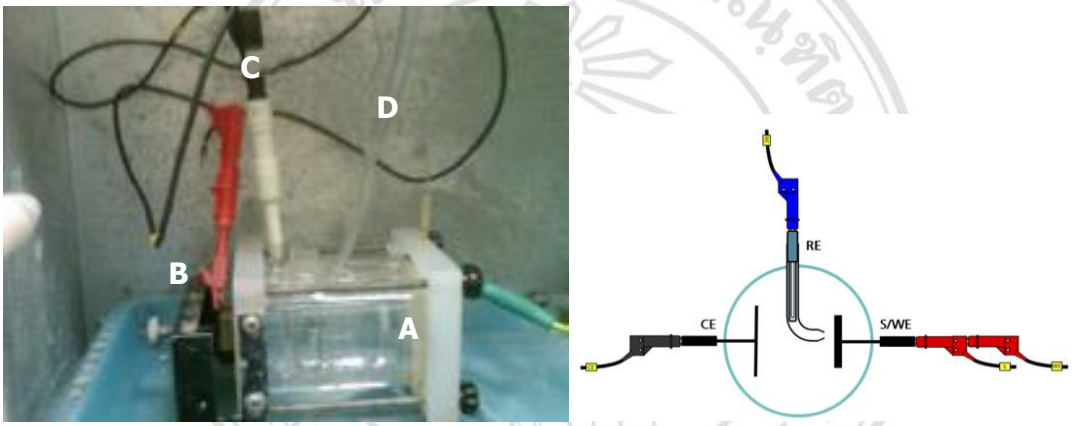

Figure 3.10 Three electrode cell for pitting corrosion resistance test:

Flat cell (A) inside a Faraday cage, specimen coupon (B) as working electrode (WE), Pt counter electrode (C), Luggin-Haber/Luggin capillary tube (D) connected to saturated calomel electrode (SCE) used as reference electrode (RE) through salt bridge connection.

To decrease Ohmic drop, Luggin-Haber/Luggin capillary was used as such to bring the RE to be closed to almost zero distance from the surface of the WE through a salt bridge of KCl 3.5 mol/l. Leakage current is considered to be as low as a few pA, since there is no voltage drop across the capillary. Autolab P302 potentiostat/galvanostat was utilized. Cyclic potentiodynamic polarization technique had been carried out in deaerated atmosphere with a scan rate at 1.667 mV/sec. Before starting corrosion test, samples with exposure area to electrolyte of 0.789 cm^2 had been left to equilibrium stage in electrolyte at open circuit potential (OCP) of -300 mV_{SCE} at

24 ±2 degree Celsius for 30 minute. Scanning was cathodically applied at potential from -1000 to 300 mVSCE and anodically reversed to -300 mV_{SCE}. Corrosion potential (E_{corr}), corrosion current density (I_{corr}), corrosion rate, break down potential (E_b), passive potential (E_p) and repassivation potential (E_b-E_p) were determined from cyclic potentiodynamic polarization curve and Tafel plot. Average results were obtained from 3 to 5 runs as to ensure test accuracy.

Specimen preparation and inspection after pitting corrosion resistance test followed ASTM Practice G1-03, G46-03 and G61-03. Pit morphology was observed by microscopic techniques. Calculation of pit volume density distribution of pits was based on optical microscopy observation as illustrated in Figure 3.11. Micrographs were captured using an Olympus BH2-UMA optical microscope at a magnification of x50 and pit width and volume density were measured by Image Pro PlusVer 5.1.0.20 image analysis software. Pit depth was measured by Dewinter Material Plus 4.1 unit attached to Meiji Keyence LK-G82 optical microscope at a magnification of x200.

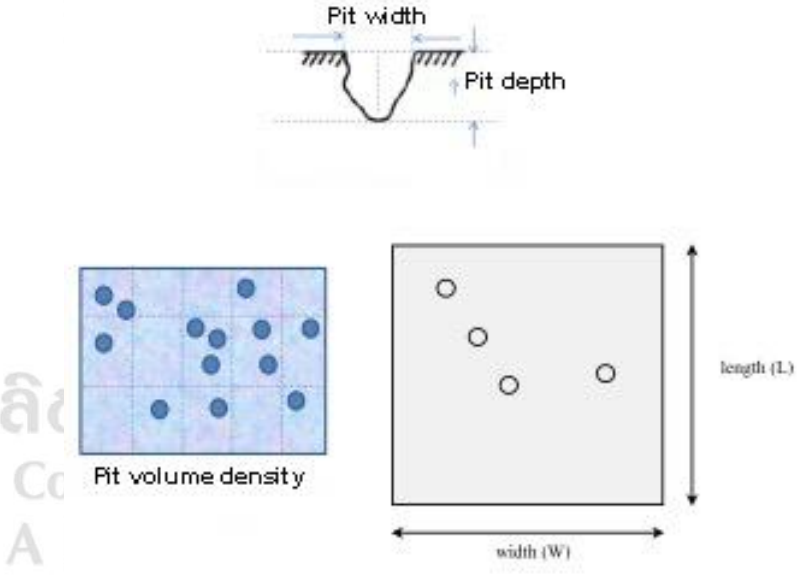

Figure 3.11 Pit morphology observations in terms of width, depth and volume density

3.10 Degree of Sensitization Test

Specimens for degree of sensitization (DOS) test were cut at a distance around 2 mm from both sides of the weld center line and prepared as for pitting corrosion resistance test. They were kept at room temperature in a vacuum desiccator for at least 24 hours prior to be attached to flat cell as working electrode, labelled (B) in a typical 3-electrode cell as shown in Figure 3.10. Each specimen with exposure area of 0.789 cm^2 was allowed to stabilize in the solution of 0.5 M H_2SO_4 + 0.01 M KCN (starting pH around 3 and deaerated in single wall flat cell with oxygen flow and with nitrogen flush in double wall flat cell) at an open circuit potential around -300 mV for 30 minutes before passivation at -500 mV for 1 min. Scanning was started from -500 to +200 mV_{SCE} and then reversed back to -500 mV_{SCE} with a scan rate at 1.667 mV/sec. Test parameters in the present work followed the work by Záhumenský *et al*. (1999), Sidhom *et al*. (2007) and Metikoš-Huković *et al*. (2011). Double loop potentiodynamic reactivation (DLEPR) generated from forward and reverse scans of cyclic potentiodynamic curve is used to estimate the degree of sensitization (DOS) of test coupons. The calculated ratio between peak current density during reactivation I_r and activation $I_a(I_r/I_a)$following Rahimi *et al*. (2010 and 2011) is used as the evaluation basis. Observation of grain boundaries was performed by microscopic techniques.

ASTM E112 grain-size number (G) to be used for the normalized charge (P_a) calculation can be obtained from the line-intercept method. Micrographs of grain morphology at 5 random areas were obtained from optical microscopy at a magnification x200 to determine average G values.

3.11 Micro-Vickers Hardness of Weldment

To performed micro-Vickers hardness (MVH) test, welded specimens were polished down to 1 micron diamond paste. Measurement was conducted at room temperature (22 ^{o}C) with an applied force of 0.2 kgf and dwell time of 20 s by Anton Paar, PaarPhysica, MHT-10 micro-hardness tester, equipped with a Sony CCD YS-W150, LEICA optical microscope and image analysis software as shown in Figure 3.12.

(a) (b)

Figure 3.12

(a) Vickers indenter, (b) Anton Paar, PaarPhysica, MHT-10 micro-hardness tester, equipped with a Sony CCD YS-W150, LEICA optical microscope andimage analysis software

3.12 Tensile Test

To minimize the effect of stress-induce during sample preparation, wire-cut method has been selected for cutting of base austenitic stainless steels and PCTIGW sheets to prepare dog bone shape specimens as illustrated in Figure 3.13. Instron 8872 Universal Testing Machine was selected to performed tensile test at a test speed of 5 mm/min and a maximum load of 1000N, adapted from the work by Kumar and Shahi, (2011).

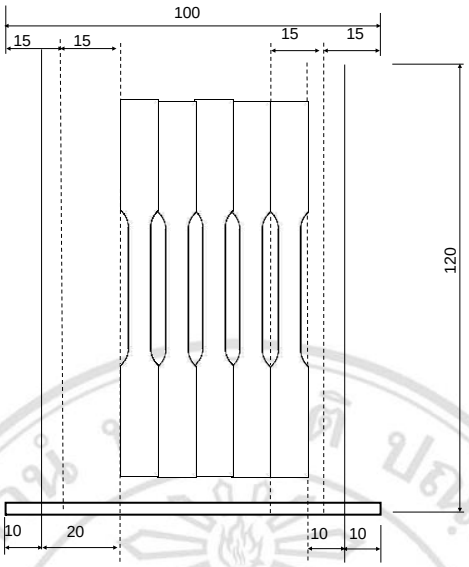

(a)

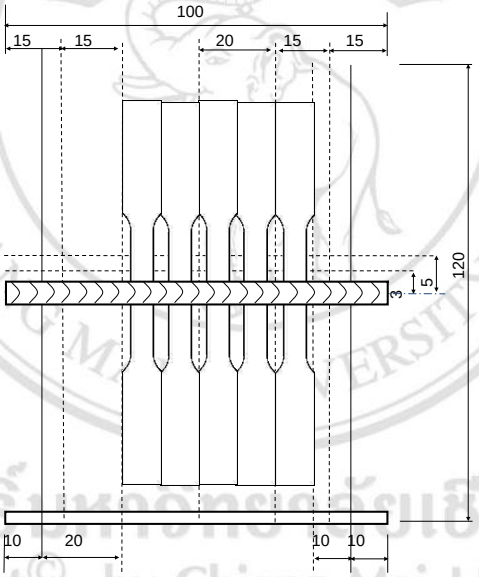

(b)

Figure 3.13 Illustration of dog bone specimens for tensile test: